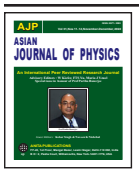

Asian Journal of Physics
Vol. 31, Nos 11-12 (2022) 1027-1034
Available on: www.asianjournalofphysics.com

ap

Digital refocusing of images recorded with white light using Lucy-Richardson-Rosen algorithm

P A Praveen[1], A Bleahu[1], F G Arockiaraj[1,2], S Gopinath[1,3], D Smith[4], S H Ng[4], A S J F Rajeswary[1], Saulius Juodkazis[4,5] and Vijayakumar Anand[1,4]

[1]*Institute of Physics, University of Tartu, W. Ostwaldi 1, 50411 Tartu, Estonia.*

[2]*PG & Research Department of Physics, The American College, Madurai- 625 009, India*

[3]*PG & Research Department of Physics, Thiagarajar College, Madurai- 625 002, India*

[4]*Optical Sciences Center, Swinburne University of Technology, Melbourne 3122, Australia*

[5]*Tokyo Tech World Research Hub Initiative* (*WRHI*), *School of Materials and Chemical Technology, Tokyo Institute of Technology, 2-12-1, Ookayama, Meguro-ku, Tokyo 152-8550, Japan*

Dedicated to Professor Partha Banerjee for his enormous contributions to the advancement of research and education in holography through his unique vision and outstanding dedication

Lens-based imaging is one of the widely used scientific methods to record optical information. As long as the imaging conditions are satisfied, this method can be used to image an object faithfully. However, beyond the limit of the depth of focus of the optical element, the collected image appears blurred. Though shifting the location of the optical element or the sensor offers a solution to the above problem, it is not suitable for recording dynamic events. There are different deconvolution methods available for digital refocusing of blurred images. Recently, a new reconstruction method called Lucy-Richardson-Rosen algorithm (LR^2A) was developed for deconvolution based 2D and 3D incoherent imaging applications. In the present work, we have demonstrated LR^2A on blurred images recorded using white light for the first time. A simple, commonly available refractive lens along with an incoherent white light source was used to record the point spread functions (PSF) at different depths. Then, the object information in the corresponding planes were also recorded. Finally, the PSF library was used to digitally refocus the object information. The results were compared with standard algorithms such as Lucy-Richardson and nonlinear reconstruction methods. In all the cases, LR^2A exhibited a superior performance.

Keywords: Deblurring, Computational imaging, Lucy-Richardson-Rosen Algorithm, Incoherent imaging.

1 Introduction

An incoherent source is a better choice for imaging due to many advantages such as higher imaging resolution, easy availability, eye-safe, low-cost, and minimal imaging noises in comparison to coherent sources [1]. Incoherent imaging methods have a wide applicability including imaging of astronomical and fluorescence objects [2]. Even though incoherent imaging in 2D is simple and well-established, much improvement and dedicated research is required for 3D incoherent imaging. Incoherent 3D imaging can be broadly classified into two types (i) holography and (ii) deconvolution. As is known, holography-based 3D imaging methods require two-wave interference, often leading to a complex optical setup followed by a computational reconstruction of the recorded hologram [3-6]. Few notable systems in this domain are

Corresponding author
e mail: vijayakumar.anand@ut.ee (Vijayakumar Anand)

rotational shearing interferometer [7], conoscopic holography [8], Fresnel incoherent correlation holography [9,10], Fourier incoherent single channel holography [11], and coded aperture correlation holography [12]. In case of of deconvolution, the linearity conditions of incoherent imaging can be used along with the computational deconvolution methods to reconstruct the images in 3D. The setup is simple and does not require two-beam interference, vibration isolation systems, or any other complex accessories. Due to the above facts, deconvolution-based approaches are considered simpler, faster, and economical than the holography counterparts. In deconvolution-based imaging, it is necessary to prerecord point spread functions (PSFs) at all axial planes, which is one of the procedures not required in holography. The recorded object intensity is processed with the PSFs using computational deconvolution methods to reconstruct the 3D image of the object.

The deconvolution-based methods also have certain limitations and the major requirement is the availability of good computational algorithm with suitable computational power in addition to the requirement to pre-record PSFs. Due to the above reasons, even though the idea of 2D deconvolution imaging was reported in the 20th century [13,14], most significant literature appeared only in the last five years [15-17]. In the recent reports, a diffuser was often used as the optical modulator between the source and the sensor. The requirement of the diffuser arises mainly due to the requirement of the reconstruction algorithms which is a sharp autocorrelation function [18,19]. The scattered intensity distribution from the diffusers generates a sharp autocorrelation function as the average speckle size equals the diffraction limited spot size ~λ/NA, where NA is the numerical aperture. Therefore, the autocorrelation function is twice that of the diffraction limited spot size ~2λ/NA. A recent computational reconstruction method called non-linear reconstruction (NLR) was able to obtain a computational resolution equal to the diffraction limited spot size. However, one of the challenges in using a diffuser is the low SNR, which prevents a broader applicability of this interesting 3D imaging method. So, it is necessary to find alternative optical fields that would have better SNR and focus light in a small area of the sensor.

Recently, the possibility of applying deterministic optical fields instead of scattered field for deconvolution-based imaging application was investigated [20]. Many deterministic fields were found to be suitable for indirect incoherent imaging applications when NLR was applied. In the present work, we have used a simple refractive lens along with a white light incoherent source to demonstrate the 3D imaging of test objects. For this purpose, a recently developed Lucy-Richardson-Rosen algorithm (LR^2A) was used for the image reconstruction [21]. This algorithm is a combination of well-known Lucy-Richardson algorithm (LRA) and NLR [21,22]. This improved method has already proven efficient in the case of micro-spectroscopy and single wavelength optical deep deconvolution studies. In this work, we have shown that the algorithm is capable of reconstruction of object information with broadband incoherent source –with low spatial as well as low temporal coherence. The methods, results, and corresponding discussions are presented in the following sections.

2 Method

A schematic of the optical configuration is given in Fig 1. A white LED light with negligible spatial or temporal coherence was used as the source. A point object generates a total amplitude $\sqrt{\int_{\lambda_1}^{\lambda_2} I_o(\lambda)\, d\lambda}$ for a broadband source with wavelength limits of λ_1 and λ_2. Considering a single wavelength from a point located at $\bar{r}_o = (x_o, y_o)$, a complex amplitude $C_1 \sqrt{I_o(\lambda)}\, Q\left(\frac{1}{z_s}\right) L\left(\frac{\bar{r}_o}{z_s}\right)$ is generated at the plane of the refractive lens located at a distance z_s from it, where λ is the wavelength of the source used, $Q(1/z_s) = \exp[j\pi R^2/\lambda_s]$ and $L(\bar{o}/z_s) = \exp[j2\pi (o_x x + o_y y)/\lambda z_s]$ are the quadratic and linear phase factors, respectively, R is the radial coordinate, $R = \sqrt{x^2 + y^2}$, and C_1 is a complex constant. The focal length f of the refractive lens can be given by $1/f = 1/z + 1/z_h$,, where

z_h is the distance between the refractive lens and the sensor plane and z is the ideal distance required between the object plane and the lens in order to satisfy the imaging condition. The complex amplitude just after the lens is $C_1 \sqrt{I_o(\lambda)}\; Q\left(\frac{1}{z_1}\right) L\left(\frac{\bar{r}_o}{z_s}\right)$, where, $z_1 = z_s f/(f - z_s)$. The intensity distribution obtained at the sensor plane located at a distance z_h from the lens is given by,

$$I_{PSF}(\bar{r}_s; \bar{r}_o, z_s, \lambda) = |C_2 \sqrt{I_o(\lambda)}\; L(\bar{r}_o/z_s)\, Q(1/z_1) \otimes Q(1/z_h)|^2 \tag{1}$$

where, $\otimes$ is a 2D convolutional operator, C_2 is a complex constant, and $\bar{r}_s$ is the location vector in the sensor plane along the transverse direction. In an ideal situation, the imaging condition is $z_s = z$ to obtain a point image on the sensor. In such a case, the lateral and axial resolutions can be given as $1.22\,\lambda z_s/D$ and $\sim 8\lambda(z_s/D)^2$, respectively. Here, D is the diameter of the lens and the magnification of the system is given by $M = z_h/z_s$.

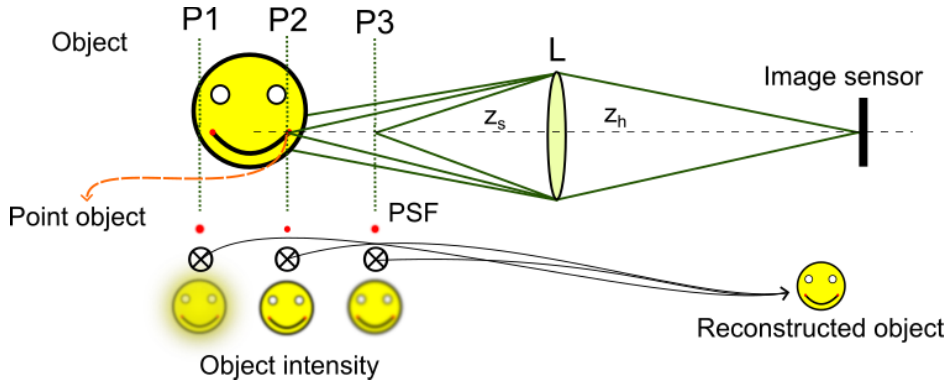

Fig 1. Schematic of the optical configuration used for the experiment. P1, P2, and P3 correspond to different object planes.

The total intensity recorded by the image sensor is given as

$$I_{PSF}(\bar{r}_s; \bar{r}_o, z_s) = \int_{\lambda_1}^{\lambda_2} I_{PSF}(\bar{r}_s; \bar{r}_o, z_s, \lambda)\, d\lambda. \tag{2}$$

The above equation can be modified as

$$I_{PSF}(\bar{r}_s; \bar{r}_o, z_s) = I_{PSF}\left(\bar{r}_s - \frac{z_h}{z_s}\bar{r}_o; 0, z_s\right). \tag{3}$$

A 2D object can be considered as a collection of points given as

$$O(\bar{r}_o) = \Sigma_i\, a_i\, \delta(r - r_i), \tag{4}$$

where a is the amplitude. The object intensity pattern at the sensor is the summation of shifted point spread functions which can be expressed as

$$I_O(\bar{r}_s, z_s) = \sum_i a_i\, I_{PSF}\left(\bar{r}_s - \frac{z_h}{z_s}\overline{r_{o,i}}; 0, z_s\right) \tag{5}$$

Using the linearity condition for the incoherent imaging and assuming insignificant chromatic aberration as the optical modulator is a refractive lens as opposed to a diffractive element, the object intensity distribution for an object O can be reconstructed using cross-correlation given as

$$\begin{aligned} P(\bar{r}_R) &= \iint I_o(\bar{r}_o; z_s)\, I^*_{PSF}(\bar{r}_o - \bar{r}_R; z_s)\, d\bar{r}_o \\ &\iint \sum_i a_i\, I_{PSF}\left(\bar{r}_o - \frac{z_h}{z_s}\bar{r}_{s,i}; z_s\right)\, I^*_{PSF}(\bar{r}_o - \bar{r}_R; z_s)\, d\bar{r}_o \\ &\sum_i a_i\, \Lambda\left(\bar{r}_R - \frac{z_h}{z_s}\bar{r}_{s,i}\right) \approx O\left(\frac{z_h}{z_s}\bar{r}_R\right) \end{aligned} \tag{6}$$

In direct imaging mode, the object information was sampled by the lateral resolution of the system, i.e., I_O is obtained by sampling O with I_{PSF}. But when the imaging conditions are not satisfied I_{PSF} would be blurred and so is the object information. In the case of indirect imaging mode, the idea is to extract O from I_O using I_{PSF} as described above or simply $I_R = I_O * I_{PSF}$, where '$*$' is a 2 D correlation operator. The above equation can be written as $I_R = I_{PSF} \otimes O * I_{PSF}$ and can be rearranged as $I_R = O \otimes I_{PSF} * I_{PSF}$. By this way, the object information can be obtained by autocorrelating I_{PSF} and using it to sample O. The computational reconstruction method NLR can be given as,

$$I_R = \mathcal{F}^{-1}\{|\tilde{I}_{PSF}|^{\alpha} \exp[j \cdot arg(\tilde{I}_{PSF})]|\tilde{I}_O|^{\beta} \exp[-j \cdot arg(\tilde{I}_O)]\}, \tag{7}$$

where α and β are varied between –1 and 1 until a minimum background noise is obtained. Essentially, the optimal NLR would reduce the background noise arising due to the positive nature of the I_{PSF}. The performance of NLR is sometimes affected by the nature of the intensity distribution especially when the I_{PSF} is a blurred spot. Our recent studies indicated that NLR is suitable when the intensity distribution has isolated points [20,22]. In the case of blurred images, NLR is not an ideal reconstruction method. In this study, LR^{2}A is used which can be described as follows. The $(n+1)^{th}$ reconstructed image can be obtained by

$$I_R^{n+1} = I_R^n \left\{ \frac{I_O}{I_R^n \otimes I_{PSF}} \otimes I_{PSF'} \right\}, \tag{8}$$

where $I_{PSF'}$ is the complex conjugate of the I_{PSF}. The loop begins with an initial guess solution and iterates the next solution by a forward convolution and backward correlation. As seen above, the ratio of I_O and forward convolution - $I_R^n \otimes I_{PSF}$ is cross-correlated with I_{PSF} using an NLR is multiplied to the previous solution to obtain the next solution. The replacement of regular correlation by NLR improves the speed of convergence by more than 10 times in many cases and a better estimation of solution.

3 Results

The setup used for the experiment is shown in Fig 2. It consists of a spatially incoherent white LED light as the source. The object was critically illuminated by the source through an iris and a refractive lens (L1) of focal length 35 mm. A refractive lens (L2) with a focal length 50 mm was placed at 2f configuration between the test object and the image sensor (Zelux CS165MU/M 1.6 MP monochrome CMOS camera, 1440×1080 pixels with pixel size < 3.5 µm) to achieve a magnification of 1.

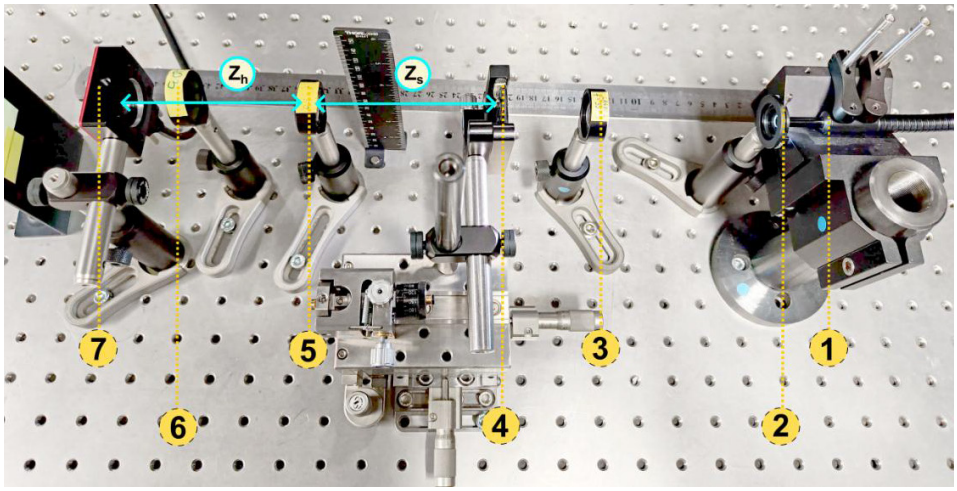

Fig 2. Experimental setup: (1) White LED, (2) Iris, (3) Lens L1 (f = 3.5 mm), (4) Test object, (5) Lens L2 (f = 50 mm), (6) ND filter (ND 1.5) and Image sensor. z_s is the distance between the test object and the lens and z_h is the distance between L2 and image sensor.

This aspect avoids the need for additional calibration as the physical space of the object is directly mapped to the sensor. The lateral and axial resolutions of the system are 1.58 μm and 10.4 μm, respectively. In order to reduce the light intensity on the image sensor a neutral density filter (ND 1.5) was placed between the sensor and the lens L2.

In order to create the PSF library a pinhole of diameter 50 μm was used. The pinhole location was changed along +z to –z direction with a step size of 0.25 mm. Then the pinhole was replaced by the test objects one after the other to record the object intensity distributions.

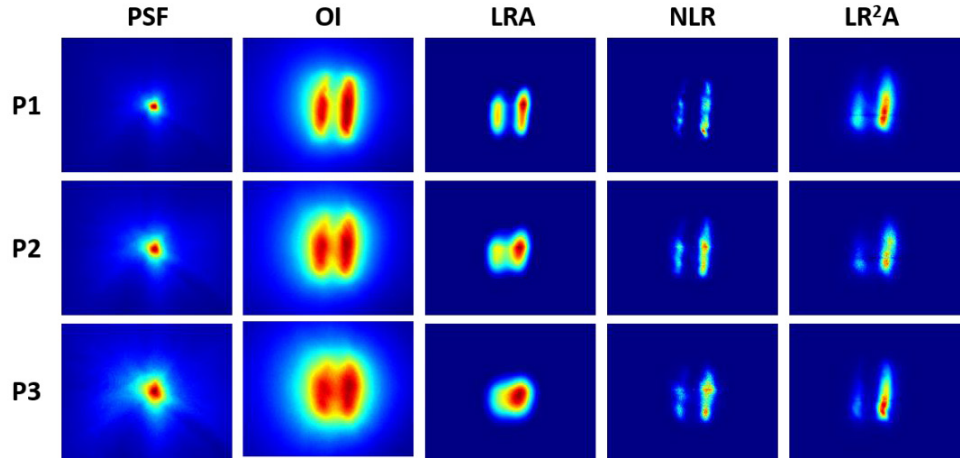

Fig 3. Images of PSF, object intensity of test object – 1, and the corresponding reconstruction results using LRA, NLR and LR^{2}A for z_s = 5, 5.2 and 5.4 cm.

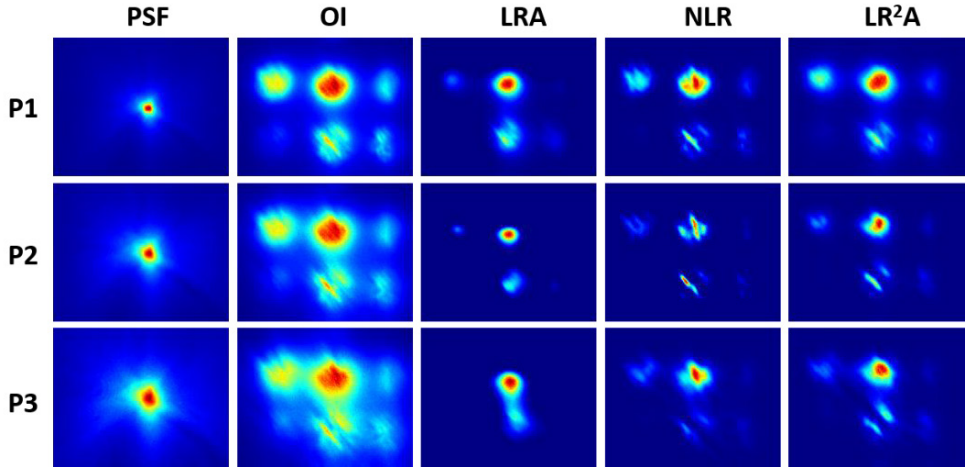

Fig 4. Images of PSF, object intensity of test object – 2, and the corresponding reconstruction results using LRA, NLR, and LR^{2}A for z_s = 5, 5.2 and 5.4 cm.

The objects were recorded at the same axial locations as the pinhole. These two data sets namely, recorded object intensities and PSF library, were then fed into the reconstruction algorithm and the images were reconstructed at different planes. Two kinds of test objects, one like a '=' sign (1.5×0.28 mm) and six concentric circles each of diameter 0.3 mm were used for the data collection. The object intensity and the PSF for both the objects were recorded at z_s = 5 cm, 5.2 cm and 5.4 cm. The recorded and reconstructed images of

test objects 1 and 2 are given in Figs 3 and 4, respectively and the parameters are as follows. For test object 1, LRA (40 iterations) for all the three planes, NLR (α = –0.2, –0.2, –0.25 and β = 0.8, 0.88, 0.88), LR^{2}A (α = –0.1, –0.1, – 0.2 and β = 0.98) with 3, 3, 4 iterations for the three planes. For test object 2, LRA (10, 40 and 30 iterations), NLR (α = –0.2, – 0.4, – 0.15 and β = 1), LR^{2}A (α = – 0.1 and β = 1) with 1, 3, 3 iterations for all the three planes. It can be seen that when the degree of blur increases, the performances of LRA and NLR are affected while LR^{2}A yields a good quality reconstructed image matching with the direct imaging results.

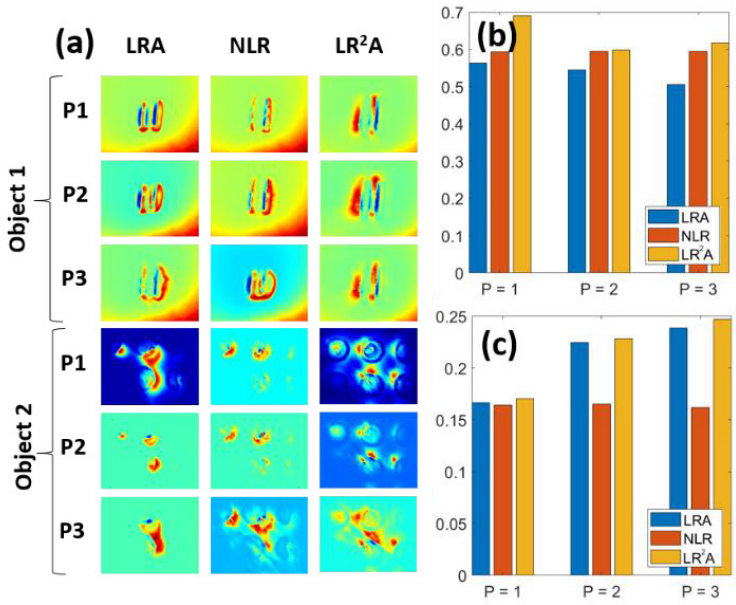

Fig 5. (a) SSIM maps of objects 1 and 2, SSIM values of the (b) object 1 and (c) object 2 for LRA, NLR and LR^{2}A.

In order to quantify and compare the results, the SSIM values are calculated for the reconstructed images using the reference image at $z_s = z$ position. The obtained values and the corresponding SSIM maps are given in Fig 5(a) and 5(b), respectively. It can be seen that in all the cases LR^{2}A performs better than LRA and NLR.

4 Conclusion

A refractive lens is one of the simplest optical components used for 2D imaging with an incoherent source. But the limitation is usually the depth of the focus which is ~λ/NA^2 and beyond that the object information is blurred [23]. There are several computational algorithms available to digitally refocus images but are limited to a small range of axial and spectral aberrations [24,25]. In this work, we have used a recently developed LR^{2}A method for deconvolution of blurred images recorded using white light and compared its results with NLR and LRA methods. In all the cases, LR^{2}A method performed better than other two methods and indicates the potential for higher dimensional imaging. If the same method was implemented using a diffractive lens instead of a refractive lens, then due to chromatic aberrations, the reconstruction results are affected. A recent study of white light imaging using a quasi-random lens with NLR showed a significantly low performance [26]. In that case, additional deep learning based denoising network was necessary to improve the reconstructed results. In this case, the same approach with a low-cost device-refractive lens and LR^{2}A method has shown improved reconstruction results. We believe that this study will lead to the development of white light-based 3D microscopy.

Acknowledgements

European Union's Horizon 2020 research and innovation programme grant agreement No. 857627 (CIPHR) and ARC Linkage LP190100505 project are acknowledged for funding. PAP, AB, ASJFR and VA thank Prof Siim Pikker, Institute of Physics, University of Tartu for the extending white LED source and Tiia Lillemaa for the administrative support.

References

1. Rosen J, Vijayakumar A, Kumar M, Rai M R, Kelner R, Kashter Y, Bulbul A, Mukherjee S, Recent advances in self-interference incoherent digital holography, *Adv Opt Photon*, 11(2019)1–66.
2. Lichtman J W, Conchello J A, Fluorescence microscopy, *Nat methods*, 2(2005)910–19.
3. Kim M K, Adaptive optics by incoherent digital holography, *Opt Lett*, 37(2012)2694–2696.
4. Liu J P, Tahara T, Hayasaki Y, Poon T C, Incoherent digital holography: a review, Appl Sci, 8(2018) Art ID:143; doi.org/10.3390/app8010143.
5. Poon T C, Optical scanning holography-a review of recent progress, *J Op. Soc* (Korea), 13(2009)406–415.
6. Rosen J, Simon A, Vijayakumar A, Jonathan A, Bouchal P, Bouchal Z, Munkh-Uchral E, Huang L, Ayumi I, Juodkazis S, Kim N, Kner P, Koujin T, Kozawa Y, Liang D, Liu J, Mann C, Marar A, Matsuda A, Nobukawa T, Nomura T, Oi R, Potcoava M, Tahara T, Thanh B L, Zhou H, Roadmap on recent progress in FINCH technology, *J Imaging*, 7(2021)197; doi.org/10.3390/jimaging7100197.
7. Murty M V R K, Hagerott E C, Rotational shearing interferometry, *Appl Opt*, 5(1966)615–619.
8. Sirat G, Psaltis D, Conoscopic holography, *Opt Lett*, 10(1985)4–6.
9. Rosen J, Brooker G, Digital spatially incoherent Fresnel holography, *Opt Lett*, 32(2007)912–914.
10. Kim M K, Incoherent digital holographic adaptive optics, *Appl Opt*, 52(2013)A117–A130.
11. Kelner R, Rosen J, Brooker G, Enhanced resolution in Fourier incoherent single channel holography (FISCH) with reduced optical path difference, *Opt Express*, 21(2013)20131–20144.
12. Vijayakumar A, Kashter Y, Kelner R, Rosen J, Coded aperture correlation holography–a new type of incoherent digital holograms, *Opt Express*, 24(2016)12430–12441.
13. Ables J G, Fourier transform photography: a new method for X-ray astronomy, *Publ Astron Soc Aust*, 1(1968)172–173.
14. Dicke R H, Scatter-hole cameras for x-rays and gamma rays, *Astrophys J*, 153(1968)L101-L106.
15. Cieślak M J, Gamage K A, Glover R, Coded-aperture imaging systems: Past, present and future development–A review, *Radiat Meas*, 92(2016)59–71.
16. Anand V, Rosen J, Juodkazis S, Review of engineering techniques in chaotic coded aperture imagers, *Light: Adv Manuf*, 3(2022) Art ID 24; doi.org/10.37188/lam.2022.024.
17. Vijayakumar A, Rosen J, Interferenceless coded aperture correlation holography–a new technique for recording incoherent digital holograms without two-wave interference, *Opt Express*, 25(2017)13883–13896.
18. Rai M R, Vijayakumar A, Rosen J, Non-linear adaptive three-dimensional imaging with interferenceless coded aperture correlation holography (I-COACH), *Opt Express*, 26(2018)18143–18154.
19. Horner J L, Gianino P D, Phase-only matched filtering, *Appl Opt*, 23(1984)812–816.
20. Smith D, Gopinath S, Arockiaraj F G, Reddy A N K, Balasubramani V, Kumar R, Dubey N, Ng S.H, Katkus T, Selva S J, Renganathan D, Kamalam M B R, Rajeswary A S J F, Navaneethakrishnan S, Inbanathan S R, Valdma S.-M, Praveen P A, Amudhavel J, Kumar M, Ganeev R A, Magistretti P J, Depeursinge C, Juodkazis S, Rosen J, Anand V, Nonlinear reconstruction of images from patterns generated by deterministic or random optical masks—Concepts and review of research, *J Imaging*, 8(2022) Art ID 174; doi.org/10.3390/jimaging8060174.
21. Anand V, Han M, Maksimovic J, Ng S H, Katkus T, Klein A R, Bambery K R, Tobin M J, Vongsvivut J, Juodkazis S, Single-shot mid-infrared incoherent holography using Lucy Richardson Rosen algorithm, *Opto-Electron Sci*, 1(2022) Art ID 210006; doi. 10.29026/oes.2022.210006.

22. Praveen P A, Gracy Arockiaraj F, Gopinath S, Smith D, Kahro T, Valdma S-M, Bleahu A, Ng S H, Reddy A N K, Katkus T, Rajeswary A S J F, Ganeev R A, Pikker S, Kukli K, Tamm A, Juodkazis S, Vijayakumar A, Deep deconvolution of object information modulated by a refractive lens using Lucy-Richardson-Rosen algorithm, *Photonics*, 9(2022)625; doi.org/10.3390/photonics9090625.
23. Wang Z, Bovik A C, Sheikh H R, Simoncelli E P, Image quality assessment: From error visibility to structural similarity, *IEEE Trans Image Process*, 13(2004)600–612.
24. Beck A, Teboulle M, Fast gradient-based algorithms for constrained total variation image denoising and deblurring problems, *IEEE Trans Image Process*, 18(2009)2419–2434.
25. Biemond J, Lagendijk R L, Merserau R M, Iterative methods for image deblurring, *Proc IEEE*, 78(1990)856–883.
26. Anand V, Ng S H, Katkus T, Juodkazis S, White light three-dimensional imaging using a quasi-random lens, *Opt Express*, 29(2021)15551–15563.

[*Received*: 02.11.2022; *accepted*: 30.12.2022]